International Journal of Thermal Sciences 49 (2010) 1288–1302

Contents lists available at ScienceDirect

International Journal of Thermal Sciences

journal homepage: www.elsevier.com/locate/ijts

Gas-phase entropy generation during transient methanol droplet combustion

Daniel N. Pope [a,*], Vasudevan Raghavan [b], George Gogos [c]

[a] University of Minnesota Duluth, Department of Mechanical and Industrial Engineering, 105 VKH, 1305 Ordean Court, Duluth, MN 55812-3042, USA
[b] Indian Institute of Technology Madras, Chennai 600036, India
[c] University of Nebraska-Lincoln, Department of Mechanical Engineering, N104 Walter Scott Engineering Center, Lincoln, NE 68588-0656, USA

ARTICLE INFO

Article history:
Received 18 June 2009
Received in revised form
23 February 2010
Accepted 28 February 2010
Available online 7 April 2010

Keywords:
Entropy generation
Droplet combustion
Methanol
Surface tension
Numerical model

ABSTRACT

A numerical model was used to investigate gas-phase entropy generation during transient methanol droplet combustion in a low-pressure, zero-gravity, air environment.A comprehensive formulation for the entropy generation in a multi-component reacting flow is derived. Stationary methanol droplet combustion in a low ambient temperature (300 K) and a nearly quiescent atmosphere was studied and the effect of surface tension on entropy generation is discussed. Results show that the average entropy generation rate over the droplet lifetime is higher for the case that neglects surface tension. Entropy generation during the combustion of methanol droplets moving in a high-temperature environment (1200 K), as seen in a typical spray combustion system, is also presented. Entropy generation due to chemical reaction increases and entropy generation due to heat and mass transfer decreases with an increase in initial Reynolds number over the range of initial Reynolds numbers (1–100) considered. Contributions due to heat transfer and chemical reaction to the total entropy generation are greater than the contribution due to mass transfer. Entropy generation due to coupling between heat and mass transfer is negligible. For moving droplets, the lifetime averaged entropy generation rate presents a minimum value at an initial Reynolds number of approximately 55.

1. Introduction

Entropy generation is a measure of the inherent irreversibility of a process. Single droplet combustion, which forms the basis for spray combustion, is highly irreversible. Thus, a thorough knowledge of entropy generation during single droplet combustion is required to improve the efficiency of a spray combustion device. Many experimental and numerical studies have been conducted in order to explore various aspects of droplet combustion. Droplet combustion experiments are well suited for determining bulk parameters such as evaporation constants and droplet lifetimes. More detailed information, such as the rate of entropy generation, can only be obtained through the use of experimentally validated numerical models.

Experimental studies on spherically symmetric fuel droplet combustion have been conducted by several investigators [1–10]. These studies use several different fuels including methanol, ethanol, n-heptane, and dodecanol. The use of methanol as a fuel in droplet combustion experiments offers several advantages: methanol does not produce soot, it has a simple chemical composition, and its oxidation mechanism is well understood. An added complication when using methanol is the continuous absorption of water into the droplet. The combined effects of increased water content within the droplet and gas-phase convection eventually leads to flame extinction. The one-dimensional analytical and numerical studies of Marchese et al. [8], Shaw [11], Zhang et al. [12], and Marchese and Dryer [13] have shown that considering only diffusion transport of water into the methanol droplet leads to extinction diameters that are much lower than the corresponding experimental results [12,13]. In addition, diffusion alone cannot account for the large quantities of water absorbed by a methanol droplet [12]. Surface tension effects can account for the enhanced transport into the droplet.

Axisymmetric numerical models for droplet combustion have also been developed and reported in the literature. Quasi-steady models have been used to simulate the low-pressure burning of fuel droplets during the period following the initial ignition and internal heating transients. These quasi-steady models are usually validated using the porous sphere experimental technique [14,15]. Several authors have conducted quasi-steady simulations to study the effect of a convective flow field on the burning rate of liquid droplets [16–18]. Pope and Gogos [19] developed a quasi-steady model with a new multi-component diffusion formulation. Pope and Gogos [20] investigated the extinction of the flame in the front

* Corresponding author. Tel.: +1 218 726 6685; fax: +1 218 726 8596.
E-mail address: dpope@d.umn.edu (D.N. Pope).

1290-0729/$ – see front matter © 2010 Elsevier Masson SAS. All rights reserved.
doi:10.1016/j.ijthermalsci.2010.02.012

Nomenclature

c_p	specific heat capacity
D_{ij}	binary diffusion coefficient for the i–j species pair
$D_{T,i}$	thermal diffusion coefficient for the ith species
D'	thermal diffusion coefficient
d	droplet diameter
$\mathbf{f}_i$	body force per unit mass
g	gravitational acceleration
H	enthalpy
h	specific enthalpy
h^0	specific heat of formation at temperature T^0
k	thermal conductivity
M	number of chemical reactions
m	mass
N	number of chemical species
n	number of moles
$\mathbf{P}$	stress tensor
p	pressure
p^0	reference pressure
$\mathbf{q}$	heat-flux vector
$\mathbf{q}_R$	radiant heat-flux vector
R_u	universal gas constant
Re	Reynolds number (dU_∞/ν_∞)
r	radial coordinate
$\mathbf{S}$	entropy generation rate (W/K)
S'	lifetime averaged entropy generation rate (W/K)
s	entropy flux vector
s	specific entropy
T	temperature
T^0	reference temperature
t	time
t_d	droplet lifetime
$\mathbf{U}$	unit tensor
U_∞	freestream velocity
u	specific internal energy
$\boldsymbol{V}_i$	diffusion velocity of the ith species
$\boldsymbol{V}_i$	component of $\boldsymbol{V}_i$ caused by all effects except temperature gradient
ν	mass-average velocity vector
$\boldsymbol{W}_i$	component of $\boldsymbol{V}_i$ caused by temperature gradient
$\overline{W}$	average molecular weight
W	molecular weight
X	mole fraction
Y	mass fraction

Greek Symbols

$\delta\boldsymbol{V}_i$	correction velocity for $\boldsymbol{V}_i$
μ	dynamic viscosity
μ_c	specific chemical potential
$\overline{\mu}_c$	molar chemical potential
ν	kinematic viscosity
Φ	viscous dissipation
ρ	density
$\overline{\rho}$	molar concentration
σ	rate of entropy generation per unit volume (W/m^3 K)
θ	polarcoordinate
ω_i	rate of species i mass production per unit volume

Subscripts

∞	freestream or outer computational boundary
μ	due to viscous dissipation
θ	polar direction
0	initial condition
c	due to coupling between heat and mass transfer
h	due to heat transfer
i	ith species
m	due to mass transfer
r	due to chemical reaction
t	total

Superscripts

T	transpose

portion of an n-heptane droplet and developed suitable correlations for the Damköhler number as a function of Reynolds number at extinction. Raghavan et al. [21] investigated the quasi-steady burning of spherical methanol particles in a mixed convective environment, for a wide range of Reynolds numbers. The burning characteristics in the presence of an envelope flame, transition flame, and a wake flame have been presented in detail. Transient models have also been employed to investigate phenomena present during methanol droplet combustion. Aharon and Shaw [22], in their numerical investigation of a bi-component droplet using an axisymmetric droplet evaporation model, have concluded that the thermal Marangoni effect (surface tension gradient due to temperature gradient) has a stabilizing effect and the solutal Marangoni effect (surface tension gradient due to composition gradient) has a destabilizing effect. Dwyer et al. [23–25] used an axisymmetric model to investigate surface tension effects for both vaporizing and combusting methanol droplets. Their results indicate that thermal and solutal Marangoni effects can greatly influence the flow patterns within a liquid droplet. The influence of the thermal Marangoni effect on droplet evaporation in a convective environment was also studied by Shih and Megaridis [26]. Their results show that surface tension gradients due to spatial variations of temperature along the interface have a profound impact on droplet dynamic behavior.

Pope et al. [27] developed a transient droplet combustion model in order to investigate the effect of forced convection on suspended as well as moving n-heptane droplets. Raghavan et al. [28] modified the transient model [27] in order to include methanol as the fuel and the effect of surface tension gradients at the interface. In their transient study within a nearly quiescent environment, they reported that a weak liquid-phase circulation introduced as a perturbation through a weak gas-phase convective flow ($\mathrm{Re} = 0.01$) is greatly enhanced due to surface tension effects. The inclusion of surface tension effects creates complex flow patterns in the droplet, which aid the absorption of water by enhancing mixing within the droplet. If surface tension effects are neglected, water absorption due to diffusion alone produces an extinction diameter much smaller than obtained experimentally. Recently, Raghavan et al. [29] have investigated the effects of surface tension and forced convection on the combustion of suspended and moving methanol droplets and have concluded that, for moving methanol droplets, surface tension effects are important regardless of the initial Reynolds number considered.

As was previously mentioned, during droplet combustion, complex chemical and transport processes that are highly irreversible take place simultaneously. These processes result in the release of chemical energy, a change in chemical composition, and the distribution of energy and chemical species via convective and diffusive transport mechanisms. The entire process is accompanied by an

irreversible increase in entropy, which leads to a decrease in exergy (available energy). The entropy generation rate should be as low as possible to minimize the destruction of exergy, and therefore maximize the available energy. Thus, the analysis of entropy generation rate becomes important [30–33]. For droplet combustion, the sources of entropy generation in flames must be identified and their relative strengths evaluated at different conditions. An expression for the entropy generation rate has been reported by Arpaci and Selamet [34]. They accounted for dissipation of thermal, mechanical, and other forms of energy on entropy generation in their study of premixed flames in a flat burner. Dash and Som [35] investigated the transport processes and associated irreversibilities for droplet combustion in a convective environment. They used results from their transient, axisymmetric numerical model to determine the instantaneous rate of entropy production and its variation with time. The relative influences of parameters such as the initial Reynolds number, the ratio of the freestream to initial droplet temperature, and the ambient pressure on the entropy generation rate during droplet combustion have been presented. Puri [36] conducted a second law analysis for a single droplet burning in a convective environment. The optimum transfer number for minimizing the entropy generation in droplet combustion was found to be directly proportional to the square of the relative velocity, and inversely proportional to the heat release and the temperature difference between the droplet surface and the surrounding gas. Hiwase et al. [37] modeled the entropy balance and performed the subsequent exergy analysis for spherically symmetric droplet combustion. They suggest that the available energy is best utilized when the initial Damköhler number is small (as close as possible to its limiting value for initiation of ignition), and ambient temperature is high. Datta and Som [38] performed a second law analysis of the spray combustion process with varying inlet pressure, temperature, and swirl. Nishida et al. [39] also analyzed entropy generation and exergy loss during combustion. An extensive parametric study of entropy generation during the quasi-steady burning of spherical methanol particles was recently performed by Raghavan et al. [40]. They have shown that entropy generation due to body forces (gravity), viscous dissipation, and coupling between heat and mass transfer are negligible when compared to contributions due to heat transfer, chemical reaction, and mass transfer. The process of flame transition had a large effect on the entropy generation rate [40].

The current study addresses the gas-phase entropy generation during the transient combustion of suspended and moving methanol droplets in a low-pressure, zero-gravity air environment. Liquid-phase entropy generation is not included in the present analysis because: 1) the droplet temperature is almost uniform after a very short initial ignition transient during which the temperature varies from 298 K at the center to 338 K (boiling pt. of methanol) at the surface – thus entropy generation due to heat transfer is negligible, and 2) only two non-reacting, perfectly miscible species (methanol and water) are present in the droplet and surface tension enhances mixing in the droplet resulting in an almost uniform species distribution – thus entropy generation due to both chemical reaction and mass transfer are negligible. A detailed expression for entropy generation in multi-component reacting mixtures is derived and compared to other formulations presented in the literature. The specific form of the expression that is used in the present study is also discussed. The velocity, pressure, temperature, and species mass fraction fields are determined using a predictive, transient, two-phase, axisymmetric model that includes surface tension effects. Calculation of the entropy generation rate occurs during post processing. Results are presented for a suspended droplet in a low-temperature, nearly quiescent environment, and for a moving droplet in a high-temperature environment. For the suspended droplet case, the results show that neglecting surface tension effects produces a higher average rate of entropy generation over the droplet lifetime. In the moving droplet case, the average rate of entropy generation over the droplet lifetime is minimized when the initial Reynolds number is approximately 55.

2. Derivation of entropy generation

The governing equations for a multi-component, reacting mixture as presented by Williams [41] are used in the following derivation. The vector form of the energy equation is

$$\rho\frac{\partial u}{\partial t}+\rho\boldsymbol{v}\cdot\nabla u = -\nabla\cdot\boldsymbol{q}-P:(\nabla\boldsymbol{v})+\rho\sum_{i=1}^{N}Y_i\boldsymbol{f}_i\cdot\boldsymbol{V}_i$$

where

$$\boldsymbol{P} = \left[p+\frac{2}{3}\mu(\nabla\cdot\boldsymbol{v})\right]\boldsymbol{U}-\mu\left[(\nabla\boldsymbol{v})+(\nabla\boldsymbol{v})^{\mathrm{T}}\right]$$

is the stress tensor, the heat-flux vector is defined by

$$\boldsymbol{q}=-k\nabla T+\rho\sum Y_i\boldsymbol{V}_i h_i+R_uT\sum_i\sum_j\left(\frac{X_jD_{T,i}}{W_iD_{ij}}\right)(\boldsymbol{V}_i-\boldsymbol{V}_j)+\boldsymbol{q}_R \quad (1)$$

and the two dots (:) imply that the tensors are to be contracted twice. The expression for the stress tensor can be rewritten as

$$\begin{aligned}\boldsymbol{P}:(\nabla\boldsymbol{v}) &= p(\nabla\cdot\boldsymbol{v})+\frac{2}{3}\mu(\nabla\cdot\boldsymbol{v})^2-\mu\left[(\nabla\boldsymbol{v})+(\nabla\boldsymbol{v})^{\mathrm{T}}\right]:(\nabla\boldsymbol{v})\\ &= p(\nabla\cdot\boldsymbol{v})-\Phi\end{aligned}$$

where

$$\Phi = -\frac{2}{3}\mu(\nabla\cdot\boldsymbol{v})^2+\mu\left[(\nabla\boldsymbol{v})+(\nabla\boldsymbol{v})^{\mathrm{T}}\right]:(\nabla\boldsymbol{v}) \quad (2)$$

is the viscous dissipation. By introducing the definition for the substantial derivative, the energy equation can be rewritten as

$$\rho\frac{Du}{Dt} = -\nabla\cdot\boldsymbol{q}-p(\nabla\cdot\boldsymbol{v})+\Phi+\rho\sum_{i=1}^{N}Y_i\boldsymbol{f}_i\cdot\boldsymbol{V}_i \quad (3)$$

Similar expressions can be written for both the continuity equation

$$\frac{D\rho}{Dt}+\rho\nabla\cdot\boldsymbol{v} = 0 \quad (4)$$

and conservation of species [41].

$$\rho\frac{DY_i}{Dt} = \omega_i-\nabla\cdot(\rho Y_i\boldsymbol{V}_i) \quad (5)$$

The diffusion velocity $\boldsymbol{V}_i$ in the conservation of energy and species equations is determined via solution of the following equation [41].

$$\begin{aligned}\nabla X_i = &\sum_{j=1}^{N}\left(\frac{X_iX_j}{D_{ij}}\right)(\boldsymbol{V}_j-\boldsymbol{V}_i)+(Y_i-X_i)\left(\frac{\nabla p}{p}\right)+\frac{\rho}{p}\sum_{j=1}^{N}Y_iY_j\left(\boldsymbol{f}_i-\boldsymbol{f}_j\right)\\ &+\sum_{j=1}^{N}\left(\frac{X_iX_j}{\rho D_{ij}}\right)\left(\frac{D_{T,j}}{Y_j}-\frac{D_{T,i}}{Y_i}\right)\left(\frac{\nabla T}{T}\right)\end{aligned} \quad (6)$$

Equation (6) states that mass diffusion consists of four components: “ordinary” diffusion, which is mass diffusion due to concentration gradients; mass diffusion due to pressure gradients; mass diffusion due to variable body forces; and “thermal” diffusion

(also known as the Soret effect), which is mass diffusion caused by temperature gradients.

2.1. Entropy generation for an ideal gas mixture

The method described by Hirschfelder et al. [30] is employed to derive the entropy generation term. The change in specific internal energy (u) in J/kg can be related to the change in specific entropy (s) in J/(kg K) via the Gibbs equation:

$$Tds = du + pd\left(\frac{1}{\rho}\right) - \sum_i \overline{\mu}_{c,i}\, d\left(\frac{n_i}{m}\right)$$

where n_i is the number of moles of the ith species in kmol, m is the total mixture mass in kg, and $\overline{\mu}_{c,i}$ is the molar chemical potential of the ith species in units of J/kmol. The number of moles and the total mass are related to the mass fraction of the ith species Y_i via $n_i/m = Y_i/W_i$ where W_i is the molecular weight of the ith species. Thus the Gibbs equation can be rewritten as

$$Tds = du + pd\left(\frac{1}{\rho}\right) - \sum_i \mu_{c,i}\, dY_i$$

where $\mu_{c,i} = \overline{\mu}_{c,i}/W_i$ is the specific chemical potential in units of J/kg. The Gibbs equation applies for any differential change in the applicable parameters, therefore one can write

$$T\frac{Ds}{Dt} = \frac{Du}{Dt} - \frac{p}{\rho^2}\frac{D\rho}{Dt} - \sum_i \mu_{c,i}\frac{DY_i}{Dt} \tag{7}$$

Substituting the conservation Eqs. (3)–(5) into Eq. (7), and multiplying the result by ρ/T gives:

$$\rho\frac{Ds}{Dt} = -\frac{1}{T}\nabla\cdot\boldsymbol{q} + \frac{\Phi}{T} + \frac{\rho}{T}\sum_i Y_i\boldsymbol{f}_i\cdot\boldsymbol{V}_i - \frac{1}{T}\sum_i \mu_{c,i}[\omega_i - \nabla\cdot(\rho Y_i\boldsymbol{V}_i)] \tag{8}$$

At this point, it is convenient to rewrite the preceding equation using the identities

$$-\frac{1}{T}\nabla\cdot\boldsymbol{q} = -\nabla\cdot\left(\frac{\boldsymbol{q}}{T}\right) - \frac{\boldsymbol{q}}{T^2}\cdot\nabla T \tag{9}$$

and

$$\frac{1}{T}\sum_i \mu_{c,i}\nabla\cdot(\rho Y_i\boldsymbol{V}_i) = \nabla\cdot\frac{1}{T}\sum_i(\mu_{c,i}\rho Y_i\boldsymbol{V}_i) + \frac{1}{T^2}\sum_i(\mu_{c,i}\rho Y_i\boldsymbol{V}_i)\cdot\nabla T - \frac{1}{T}\sum_i \rho Y_i\boldsymbol{V}_i\cdot\nabla(\mu_{c,i}) \tag{10}$$

Substituting Eqs. (9) and (10) into Eq. (8) gives

$$\rho\frac{Ds}{Dt} = -\nabla\cdot\left[\left(\frac{\boldsymbol{q}}{T}\right) - \frac{1}{T}\sum_i \mu_{c,i}\rho Y_i\boldsymbol{V}_i\right] - \frac{\boldsymbol{q}}{T^2}\cdot\nabla T + \frac{\Phi}{T} + \frac{\rho}{T}\sum_i Y_i\boldsymbol{f}_i\cdot\boldsymbol{V}_i - \frac{1}{T}\sum_i \mu_{c,i}\omega_i + \frac{1}{T^2}\sum_i(\mu_{c,i}\rho Y_i\boldsymbol{V}_i)\cdot\nabla T - \frac{1}{T}\sum_i \rho Y_i\boldsymbol{V}_i\cdot\nabla(\mu_{c,i}) \tag{11}$$

The equation of change for entropy is given by Hirschfelder et al. [30] as

$$\rho\frac{Ds}{Dt} = -\nabla\cdot\boldsymbol{s} + \sigma \tag{12}$$

where s is the specific entropy, $\mathbf{s}$ is the flux vector representing the reversible flow of entropy, and σ is the rate of irreversible production of entropy per unit volume. Comparing Eqs. (11) and (12) leads to the expressions

$$\boldsymbol{s} = \left(\frac{\boldsymbol{q}}{T}\right) - \frac{1}{T}\sum_i \mu_{c,i}\rho Y_i\boldsymbol{V}_i$$

and

$$\sigma = -\frac{\boldsymbol{q}}{T^2}\cdot\nabla T + \frac{\Phi}{T} + \frac{\rho}{T}\sum_i Y_i\boldsymbol{f}_i\cdot\boldsymbol{V}_i - \frac{1}{T}\sum_i \mu_{c,i}\omega_i + \frac{1}{T^2}\sum_i(\mu_{c,i}\rho Y_i\boldsymbol{V}_i)\cdot\nabla T - \frac{1}{T}\sum_i \rho Y_i\boldsymbol{V}_i\cdot\nabla(\mu_{c,i})$$

The preceding equation can be placed into a form similar to that given by Carrington and Sun [33]:

$$\sigma = -\frac{\boldsymbol{q}}{T^2}\cdot\nabla T + \frac{\Phi}{T} + \frac{1}{T}\sum_i \rho Y_i\boldsymbol{V}_i\cdot\left(\boldsymbol{f}_i + \frac{\mu_{c,i}}{T}\nabla T - \nabla\mu_{c,i}\right) - \frac{1}{T}\sum_i \mu_{c,i}\omega_i \tag{13}$$

The terms on the right-hand side of Eq. (13) represent the irreversibilities due to heat transfer, viscous dissipation, mass transfer, and chemical reactions, respectively. We are primarily concerned with entropy generation and therefore we will focus on Eq. (13). In particular, let us redefine the heat flux given by Eq. (1) as being composed of two parts:

$$\boldsymbol{q} = \boldsymbol{q}' + \rho\sum Y_i\boldsymbol{V}_i h_i \tag{14}$$

where the expression

$$\boldsymbol{q}' = -k\nabla T + R_u T\sum_i\sum_j\left(\frac{X_j D_{T,i}}{W_i D_{ij}}\right)(\boldsymbol{V}_i - \boldsymbol{V}_j) + \boldsymbol{q}_R \tag{15}$$

contains the components due to heat conduction, the Dufour effect, and radiation, respectively. Thus the entropy generation becomes:

$$\sigma = -\frac{\boldsymbol{q}'}{T^2}\cdot\nabla T + \frac{\Phi}{T} + \frac{1}{T}\sum_i \rho Y_i\boldsymbol{V}_i\cdot\left[\boldsymbol{f}_i + \frac{(\mu_{c,i} - h_i)}{T}\nabla T - \nabla\mu_{c,i}\right] - \frac{1}{T}\sum_i \mu_{c,i}\omega_i \tag{16}$$

For a mixture of ideal gases, the term $(h_i - \mu_{c,i})$ in the above equation is related to the partial specific entropy of the ith species (s_i) via $Ts_i = (h_i - \mu_{c,i})$. The resulting equation for entropy generation is

$$\sigma = -\frac{\boldsymbol{q}'}{T^2}\cdot\nabla T + \frac{\Phi}{T} + \frac{1}{T}\sum_i \rho Y_i\boldsymbol{V}_i\cdot[\boldsymbol{f}_i - s_i\nabla T - \nabla\mu_{c,i}] - \frac{1}{T}\sum_i \mu_{c,i}\omega_i \tag{17}$$

According to Carrington and Sun [33], the temperature gradient in the diffusion term of the above equation does not indicate coupling between heat and mass transfer. The chemical potential is defined by $\mu_{c,i} = h_i - Ts_i$ and thus, the gradient can be expressed as

$$\nabla\mu_{c,i} = \nabla h_i - T\nabla s_i - s_i\nabla T \tag{18}$$

Substituting Eq. (18) into Eq. (17) yields:

$$\sigma = -\frac{\boldsymbol{q}'}{T^2}\cdot\nabla T + \frac{\Phi}{T} + \frac{1}{T}\sum_i \rho Y_i\boldsymbol{V}_i\cdot\left[\boldsymbol{f}_i - \nabla h_i + T\nabla s_i\right] - \frac{1}{T}\sum_i \mu_{c,i}\omega_i \tag{19}$$

The specific enthalpy h_i for an ideal gas is calculated using

$$h_i = h_i^0 + \int_{T^0}^{T} c_{p,i}\, dT$$

where h_i^0 is the heat of formation of the ith species per unit mass evaluated at the reference temperature T^0, and $c_{p,i}$ is the specific heat capacity of the ith species. The partial specific entropy s_i for an ideal gas is given by

$$s_i = s_i^0 + \int_{T^0}^{T} \frac{c_{p,i}}{T} dT - R_i \ln\left(\frac{p_i}{p^0}\right) = s_i^0 + \int_{T^0}^{T} \frac{c_{p,i}}{T} dT - R_i \ln\left(\frac{p}{p^0}\right) - R_i \ln X_i$$

where s_i^0 is the specific entropy of the ith species evaluated at the reference temperature T^0 and pressure p^0, $R_i = R_u/W_i$ is the specific gas constant of the ith species, and $p_i = X_i p$ is the partial pressure of the ith species. If the ideal-gas equation of state is also employed, the gradients in the diffusion term of the entropy generation Eq. (19) can be written as

$$-\nabla h_i + T\nabla s_i = -\frac{1}{\rho_i}(p\nabla X_i + X_i \nabla p) \tag{20}$$

Substituting the above into the entropy generation equation gives:

$$\sigma = -\frac{\boldsymbol{q}'}{T^2}\cdot\nabla T + \frac{\Phi}{T} + \frac{1}{T}\sum_i \rho Y_i \boldsymbol{V}_i \cdot \left[\boldsymbol{f}_i - \frac{1}{\rho_i}(p\nabla X_i + X_i\nabla p)\right] - \frac{1}{T}\sum_i \mu_{c,i}\omega_i \tag{21}$$

Equation (21) may be used to calculate the rate of entropy generation per unit volume in a mixture of ideal gases. The terms on the right-hand side of the equation result from heat transfer (conduction, Dufour effect, and radiation), viscous dissipation, mass transfer, and chemical reactions, respectively. It should be noted here that portions of the heat and mass transfer terms express the coupling between these two phenomena.

2.2. Heat-mass transfer coupling

The total rate of entropy generation per unit volume σ for a multi-component, reacting mixture of ideal gases can be divided into five different generation terms: a heat transfer term σ_h, a mass transfer term σ_m, a heat-mass transfer coupling term σ_c, a viscous dissipation term σ_μ, and a chemical reaction term σ_r.

$$\sigma = \sigma_h + \sigma_m + \sigma_c + \sigma_\mu + \sigma_r \tag{22}$$

The coupling between heat and mass transfer is given via the Dufour and Soret effects. The Dufour effect, which is contained in the $\mathbf{q}'$ term of the entropy generation equation, represents the heat flux generated by mass diffusion. The Soret effect, which is contained in the diffusion velocity Eq. (6), represents mass diffusion caused by temperature gradients. Pope and Gogos [19] showed that, when diffusion due to pressure gradients and variable body forces is negligible, the total diffusion velocity of the ith species $\boldsymbol{V}_i$ may be written as

$$\boldsymbol{V}_i = V_i + \boldsymbol{W}_i \tag{23}$$

where $\boldsymbol{W}_i$ is the component due to "thermal" diffusion (Soret effect), and $\boldsymbol{V}_i$ is the component due to "ordinary" diffusion. For the present discussion, the effect of pressure gradients and variable body forces may be lumped with the "ordinary" diffusion velocity without any loss of generality. The resulting equations for calculating $\boldsymbol{V}_i$ would differ slightly from those given by Pope and Gogos [19]. The thermal diffusion velocity is given by

$$\boldsymbol{W}_i = -\frac{D_{T,i}}{\rho Y_i}\frac{\nabla T}{T} \tag{24}$$

which satisfies the constraint

$$\sum_{i=1}^{N} Y_i \boldsymbol{W}_i = 0 \tag{25}$$

The sum of the "ordinary", pressure gradient, and body force diffusion velocities are subject to the constraint

$$\sum_{i=1}^{N} Y_i V_i = 0 \tag{26}$$

Substituting Eq. (23) into the diffusion flux ($\rho Y_i \boldsymbol{V}_i$) in Eq. (21) and separating the terms involving the Dufour and Soret effects yields the following definitions for the entropy generation terms:

$$\begin{aligned}
\sigma_h &= \frac{1}{T^2}(k\nabla T - \boldsymbol{q}_R)\cdot\nabla T \\
\sigma_m &= \frac{1}{T}\sum_i \rho Y_i V_i \cdot \left[\boldsymbol{f}_i - \frac{1}{\rho_i}(p\nabla X_i + X_i\nabla p)\right] \\
\sigma_c &= \frac{1}{T}\sum_i \rho Y_i \boldsymbol{W}_i \cdot \left[\boldsymbol{f}_i - \frac{1}{\rho_i}(p\nabla X_i + X_i\nabla p)\right] - \frac{R_u}{T}\sum_i\sum_j \left(\frac{X_j D_{T,i}}{W_i D_{ij}}\right) \times (\boldsymbol{V}_i - \boldsymbol{V}_j)\cdot\nabla T \\
\sigma_\mu &= \frac{\Phi}{T} \\
\sigma_r &= -\frac{1}{T}\sum_i \mu_{c,i}\omega_i
\end{aligned} \tag{27}$$

2.3. Simplifying assumptions

The cumulative effects of the application of various assumptions on the entropy generation terms is discussed in this section. The first commonly applied assumption is that gravity ($\mathbf{g}$) is the only external body force per unit mass ($\mathbf{f}_i = \mathbf{g}$). The effect of variable body force is therefore removed from the diffusion velocity Eq. (6), which becomes

$$\nabla X_i = \sum_{j=1}^{N}\left(\frac{X_i X_j}{D_{ij}}\right)(\boldsymbol{V}_j - \boldsymbol{V}_i) + (Y_i - X_i)\left(\frac{\nabla p}{p}\right) + \sum_{j=1}^{N}\left(\frac{X_i X_j}{\rho D_{ij}}\right) \times \left(\frac{D_{T,j}}{Y_j} - \frac{D_{T,i}}{Y_i}\right)\left(\frac{\nabla T}{T}\right)$$

Application of the constraint Eqs. (25) and (26), shows that the effect of body forces is removed from both the mass diffusion

$$\sigma_m = -\frac{1}{T}\sum_i \boldsymbol{V}_i \cdot (p\nabla X_i + X_i \nabla p)$$

and coupling

$$\sigma_c = -\frac{1}{T}\sum_i \boldsymbol{W}_i \cdot (p\nabla X_i + X_i\nabla p) - \frac{R_u}{T}\sum_i\sum_j \left(\frac{X_j D_{T,i}}{W_i D_{ij}}\right) \times (\boldsymbol{V}_i - \boldsymbol{V}_j)\cdot\nabla T$$

terms of the entropy generation equation.

The pressure gradient is also commonly assumed to have negligible effect on the mass diffusion. The addition of this assumption results in the following diffusion velocity equation:

$$\nabla X_i = \sum_{j=1}^{N}\left(\frac{X_i X_j}{D_{ij}}\right)(\boldsymbol{V}_j - \boldsymbol{V}_i) + \sum_{j=1}^{N}\left(\frac{X_i X_j}{\rho D_{ij}}\right)\left(\frac{D_{T,j}}{Y_j} - \frac{D_{T,i}}{Y_i}\right)\left(\frac{\nabla T}{T}\right)$$

which is identical to the formulation presented by Pope and Gogos [19]. In this case, the mass diffusion and coupling terms for the entropy generation equation become

$$\sigma_{\mathrm{m}} = -\frac{1}{T}\sum_i V_i \cdot p\nabla X_i$$

and

$$\sigma_{\mathrm{c}} = -\frac{1}{T}\sum_i \boldsymbol{W}_i \cdot p\nabla X_i - \frac{R_u}{T}\sum_i\sum_j\left(\frac{X_j D_{T,i}}{W_i D_{ij}}\right)(\boldsymbol{V}_i - \boldsymbol{V}_j)\cdot\nabla T$$

The gradients of the species mole fractions may be removed through the use of the identity $X_i = Y_i\overline{W}/W_i$, where $\overline{W}$ is the average molecular weight which is given by

$$\overline{W} = \left[\sum_j \frac{Y_j}{W_j}\right]^{-1} = \sum_j X_j W_j$$

This substitution is not performed here as it results in a rather complicated expression for the entropy generation equation. Additionally, the ideal-gas equation of state may be used to obtain

$$\sigma_{\mathrm{m}} = -\frac{\rho R_u}{\overline{W}}\sum_i V_i \cdot \nabla X_i$$

and

$$\sigma_{\mathrm{c}} = -\frac{\rho R_u}{\overline{W}}\sum_i \boldsymbol{W}_i \cdot \nabla X_i - \frac{R_u}{T}\sum_i\sum_j\left(\frac{X_j D_{T,i}}{W_i D_{ij}}\right)(\boldsymbol{V}_i - \boldsymbol{V}_j)\cdot\nabla T.$$

The thermal diffusion velocity is given by Eq. (24) and the "ordinary" diffusion velocity may be calculated using

$$V_i = -\frac{D_{im}}{Y_i}\nabla Y_i + \delta V_i \tag{28}$$

where D_{im} is the effective diffusion coefficient for the ith species into the mixture of all other species, and δV_i is a correction velocity [19]. As discussed by Williams [41] (p. 644), the Dufour effect is usually negligible even when thermal diffusion (Soret effect) is not negligible. Neglecting the Dufour effect simplifies the coupling term of the entropy generation equation.

$$\sigma_{\mathrm{c}} = -\frac{\rho R_u}{\overline{W}}\sum_i \boldsymbol{W}_i \cdot \nabla X_i$$

2.4. Comparison to literature

Carrington and Sun [33] presented a derivation of the entropy generation under two separate sets of assumptions. Both of the cases they presented were for an ideal solution with no chemical reactions ($\omega_i = 0$) and negligible radiation heat transfer ($\boldsymbol{q}_R \approx 0$). Since a mixture of ideal gases is a special case of an ideal solution, simplification of the current formulation under the same assumptions as employed by Carrington and Sun [33] should yield the same equation for entropy generation. The assumptions common to both cases result in an entropy generation term due to chemical reaction of

$$\sigma_{\mathrm{r}} = 0$$

and an entropy generation term due to heat transfer of

$$\sigma_{\mathrm{h}} = \frac{k}{T^2}(\nabla T)^2$$

2.4.1. Case 1

The first case demonstrates the use of Fick's law and involves the following assumptions [33]: the Dufour and Soret effects are negligible, the pressure gradient (and thus pressure diffusion) is negligible, external body forces are negligible, and the molar concentration ($\overline{\rho} = \rho/\overline{W}$) is constant. Neglecting both the Dufour and Soret effects removes the coupling term: $\sigma_{\mathrm{c}} = 0$. Since thermal diffusion, pressure diffusion, and diffusion due to external forces are negligible, the diffusion velocity is a function of concentration gradients only. This "ordinary" diffusion velocity was defined in ref. [33] by

$$V_i = -\frac{D_{im}}{X_i}\nabla X_i$$

When the external body forces and pressure gradient are neglected, substituting the preceding equation into the mass diffusion entropy generation term in Eq. (27) gives

$$\sigma_{\mathrm{m}} = -\frac{p}{T}\sum_i V_i \cdot \nabla X_i = \overline{\rho} R_u \sum_i \frac{D_{im}}{X_i}(\nabla X_i)^2$$

If the molar concentration is constant, σ_{m} can be rewritten as

$$\sigma_{\mathrm{m}} = R_u \sum_i \frac{D_{im}}{\overline{\rho}_i}(\nabla \overline{\rho}_i)^2$$

Thus the current formulation, under the given assumptions, yields a total volumetric rate of entropy generation of

$$\sigma = \frac{k}{T^2}(\nabla T)^2 + R_u \sum_i \frac{D_{im}}{\overline{\rho}_i}(\nabla \overline{\rho}_i)^2 + \frac{\Phi}{T}$$

which is equivalent to Eq. (45) in ref. [33] given the difference in nomenclature.

2.4.2. Case 2

The second case demonstrates heat-mass transfer coupling and involves the following assumptions [33]: a binary fluid, viscous dissipation is negligible ($\Phi \approx 0$), no external forces, uniform (constant) pressure (thus there is no pressure diffusion), and uniform (constant) density. Neglecting viscous dissipation results in $\sigma_{\mu} = 0$. In this case, the Dufour and Soret effects are retained. Fick's law is used to describe the "ordinary" diffusion velocity for a binary fluid

$$V_1 = -\frac{D_{12}}{Y_1}\nabla Y_1 \quad \text{and} \quad V_2 = -\frac{D_{21}}{Y_2}\nabla Y_2 \tag{29}$$

where $D_{12} = D_{21}$ is the binary diffusion coefficient. The thermal diffusion velocity is defined by Eq. (24) as

$$\boldsymbol{W}_1 = -\frac{D_{T,1}}{\rho Y_1}\frac{\nabla T}{T} \quad \text{and} \quad \boldsymbol{W}_2 = -\frac{D_{T,2}}{\rho Y_2}\frac{\nabla T}{T} \tag{30}$$

where $D_{T,2} = -D_{T,1}$ are the thermal diffusion coefficients. The mass diffusion and coupling terms for uniform pressure and no external body forces are given by

$$\sigma_{\mathrm{m}} = -\frac{\rho R_u}{\overline{W}}\sum_i V_i \cdot \nabla X_i$$

and

$$\sigma_{\mathrm{c}} = -\frac{\rho R_u}{\overline{W}}\sum_i \boldsymbol{W}_i \cdot \nabla X_i - \frac{R_u}{T}\sum_i\sum_j\left(\frac{X_j D_{T,i}}{W_i D_{ij}}\right)(\boldsymbol{V}_i - \boldsymbol{V}_j)\cdot\nabla T,$$

respectively, where the Dufour effect in the coupling term contains the total diffusion velocity. For a binary fluid, the mass diffusion term becomes

$$\sigma_m = -\frac{\rho R_u}{\overline{W}}(V_1\cdot\nabla X_1 + V_2\cdot\nabla X_2) \tag{31}$$

Using the identities $Y_1V_1 + Y_2V_2 = 0$, $Y_1 + Y_2 = 1$, $X_1 + X_2 = 1$, $X_1 = Y_1(\overline{W}/W_1)$, and $\overline{W} = W_1W_2/(Y_1W_2 + Y_2W_1)$, the mass diffusion term can be rewritten as

$$\sigma_m = -\frac{\rho R_u}{W_1Y_2}\left(\frac{\overline{W}}{W_2}\right)V_1\cdot\nabla Y_1 \tag{32}$$

Substituting the "ordinary" diffusion velocity given by Eq. (29) and the identity $\overline{W} = \rho/\overline{\rho}$ into Eq. (32) gives

$$\sigma_m = \frac{\rho^2 R_u D_{12}}{W_1W_2Y_1Y_2\overline{\rho}}(\nabla Y_1)^2$$

which is identical to the mass diffusion term in Eq. (61) of ref. [33]. The coupling term may be expressed as

$$\sigma_c = \sigma_c^1 + \sigma_c^2$$

where

$$\sigma_c^1 = -\frac{\rho R_u}{\overline{W}}(\boldsymbol{W}_1\cdot\nabla X_1 + \boldsymbol{W}_2\cdot\nabla X_2) \tag{33}$$

and

$$\sigma_c^2 = -\frac{R_u}{T}\left\{\frac{D_{T,1}}{W_1}\left[\frac{X_2}{D_{12}}(\boldsymbol{V}_1-\boldsymbol{V}_2)\right] + \frac{D_{T,2}}{W_2}\left[\frac{X_1}{D_{21}}(\boldsymbol{V}_2-\boldsymbol{V}_1)\right]\right\}\cdot\nabla T \tag{34}$$

Equation (33) is similar to the mass diffusion term shown in Eq. (31) and the constraint $Y_1\boldsymbol{W}_1 + Y_2\boldsymbol{W}_2 = 0$ is satisfied. Thus, we can immediately write

$$\sigma_c^1 = -\frac{\rho R_u}{W_1Y_2}\left(\frac{\overline{W}}{W_2}\right)\boldsymbol{W}_1\cdot\nabla Y_1 \tag{35}$$

Substituting the "thermal" diffusion velocity given by Eq. (30) and the identity $\overline{W} = \rho/\overline{\rho}$ into Eq. (35) gives

$$\sigma_c^1 = \frac{\rho R_u D_{T,1}}{TW_1W_2Y_1Y_2\overline{\rho}}\nabla T\cdot\nabla Y_1 \tag{36}$$

Carrington and Sun [33] introduce the thermal diffusion coefficient (D') which can be written as

$$D' = \frac{D_{T,1}}{Y_1Y_2\rho T} \tag{37}$$

Substituting Eq. (37) into Eq. (36) yields

$$\sigma_c^1 = \frac{\rho^2 R_u D'}{W_1W_2\overline{\rho}}\nabla T\cdot\nabla Y_1$$

The identities $D_{T,2} = -D_{T,1}$, $D_{21} = D_{12}$, $Y_1\boldsymbol{V}_1 + Y_2\boldsymbol{V}_2 = 0$, $Y_1 + Y_2 = 1$, and $\overline{W} = X_1W_1 + X_2W_2$, can be used with Eq. (34) to obtain the following for the second coupling term.

$$\sigma_c^2 = -\frac{R_u D_{T,1}}{TD_{12}}\frac{\overline{W}}{W_1W_2Y_2}\boldsymbol{V}_1\cdot\nabla T$$

Substituting the sum of the "ordinary" and "thermal" diffusion velocities defined by Eqs. (23)–(30), the identity $\overline{W} = \rho/\overline{\rho}$, and the thermal diffusion coefficient from Eq. (37) into the preceding equation gives

$$\sigma_c^2 = \frac{\rho^2 R_u D'}{W_1W_2\overline{\rho}}\nabla T\cdot\left[\nabla Y_1 + \left(\frac{D_{T,1}}{\rho D_{12}}\right)\frac{\nabla T}{T}\right]$$

The total coupling term obtained for the second case is therefore

$$\sigma_c = \frac{\rho^2 R_u D'}{W_1W_2\overline{\rho}}\nabla T\cdot\left[2\nabla Y_1 + \left(\frac{D_{T,1}}{\rho D_{12}}\right)\frac{\nabla T}{T}\right] \tag{38}$$

The coupling term in Eq. (61) of ref. [33] for this case contains only the first term shown in Eq. (38). The second term in Eq. (38) arises from the contribution of thermal diffusion (Soret effect) to the total diffusion velocity in the heat flux caused by the Dufour effect. Carrington and Sun [33] used only the "ordinary" diffusion velocity in their formulation for the heat flux (see Eq. (59) in ref. [33]). The neglect of this additional term does not change their order of magnitude analysis [33]. As discussed by Williams [41] (p. 637), the ratio $D_{T,1}/(\rho D_{12})$ is usually less than one-tenth for gases and slightly higher for condensed phases. Thus, when the temperature gradient is not steep, the second term in Eq. (38) is negligible compared to the first term and the formulation of Carrington and Sun [33] results. Additional insight can be obtained by noting that for the constant pressure and density assumed for the present case, the assumption of an ideal-gas mixture gives

$$\nabla T = \frac{p}{\rho R_u}\nabla\overline{W} = T\left(\frac{\overline{W}}{W_2} - \frac{\overline{W}}{W_1}\right)\nabla Y_1 \tag{39}$$

Substituting Eq. (39) into Eq. (38) results in

$$\sigma_c = \frac{\rho^2 R_u D'}{W_1W_2\overline{\rho}}\nabla T\cdot\left[2\nabla Y_1 + \left(\frac{D_{T,1}}{\rho D_{12}}\right)\left(\frac{\overline{W}}{W_2} - \frac{\overline{W}}{W_1}\right)\nabla Y_1\right] \tag{40}$$

Equation (40) indicates that, unless the molecular weights of the species differ greatly, the second term (due to thermal diffusion) contributes negligibly to the coupling term.

Using the current formulation, the total volumetric rate of entropy generation for the second case obtained is

$$\sigma = \frac{k}{T^2}(\nabla T)^2 + \frac{\rho^2 R_u D_{12}}{W_1W_2Y_1Y_2\overline{\rho}}(\nabla Y_1)^2 + \frac{\rho^2 R_u D'}{W_1W_2\overline{\rho}}\nabla T\cdot\left[2\nabla Y_1 + \left(\frac{D_{T,1}}{\rho D_{12}}\right)\frac{\nabla T}{T}\right] \tag{41}$$

As previously discussed, Eq. (41) differs only in the coupling (last) term when compared to Eq. (61) of ref. [33].

3. Numerical model

The axisymmetric, transient numerical model used in this work has been described elsewhere in detail [27–29]. The model solves the conservation of mass, momentum, species, and energy equations in both the gas and liquid phase. It includes multi-component diffusion in both phases, a comprehensive method to deal with the interface (including surface tension effects), and variation of thermo-physical properties as a function of temperature and species concentration in both phases. The numerical model has been extensively validated for both n-heptane [27], and methanol [28,29] droplet combustion. Calculation of the gas-phase entropy generation rate was added to the numerical code as a post processing step to generate results for the current work.

The problem considered is the combustion of a liquid methanol droplet in a low-pressure, zero-gravity environment of infinite expanse (Fig. 1). For a suspended droplet, the $r - \theta$ coordinate system is inertial, whereas for a moving droplet, it is non-inertial. The acceleration of the non-inertial coordinate system (dU_∞/dt) has

been included in the momentum equations. The freestream pressure (p_∞) and the freestream temperature (T_∞) are held constant. The effect of the suspension fiber is neglected when simulating suspended droplets. Other assumptions include: (1) axisymmetric, laminar flow, (2) spherical droplet shape (uniform surface regression as a result of surface-averaged vaporization and surface-averaged drag force estimates have been used in order to maintain spherical droplet shape), (3) zero coefficient of bulk viscosity, and (4) thermal radiation, pressure diffusion, Dufour effect, Soret effect in the liquid phase, viscous dissipation, and pressure work are negligible. A brief description of the numerical model is given in Appendix A.

Application of the aforementioned assumptions results in the following expression for the rate of entropy generation in the gas phase per unit volume

$$\sigma = \sigma_h + \sigma_m + \sigma_c + \sigma_r \tag{42}$$

where the individual terms are defined by

$$\begin{aligned}
\sigma_h &= \frac{k}{T^2}(\nabla T)^2 \\
\sigma_m &= -\frac{\rho R_u}{\overline{W}}\sum_i V_i \cdot \nabla X_i \\
\sigma_c &= -\frac{\rho R_u}{\overline{W}}\sum_i \boldsymbol{W}_i \cdot \nabla X_i \\
\sigma_r &= -\frac{1}{T}\sum_i \mu_{c,i}\omega_i
\end{aligned} \tag{43}$$

The "ordinary" diffusion velocity and the thermal diffusion velocity are defined by Eqs. (28) and (24), respectively. Substituting these into the mass diffusion and coupling terms in Eq. (43) gives

$$\begin{aligned}
\sigma_m &= \frac{\rho R_u}{\overline{W}}\sum_i \left(\frac{D_{im}}{Y_i}\nabla Y_i - \delta V_i\right)\cdot \nabla X_i \\
\sigma_c &= \frac{R_u}{\overline{W}T}\sum_i \frac{D_{T,i}}{Y_i}\nabla T \cdot \nabla X_i
\end{aligned} \tag{44}$$

The solution for the gas-phase temperature, velocity, and species mass fraction fields is used in Eqs. (42)–(44) to calculate the rate of entropy generation per unit volume. At any instant in time, the entropy generation rate is given by

$$S = \iint \sigma 2\pi r dr d\theta \tag{45}$$

The individual components of the rate of entropy generation per unit volume, as shown in Eq. (42), can be substituted into Eq. (45) to obtain the corresponding entropy generation rates.

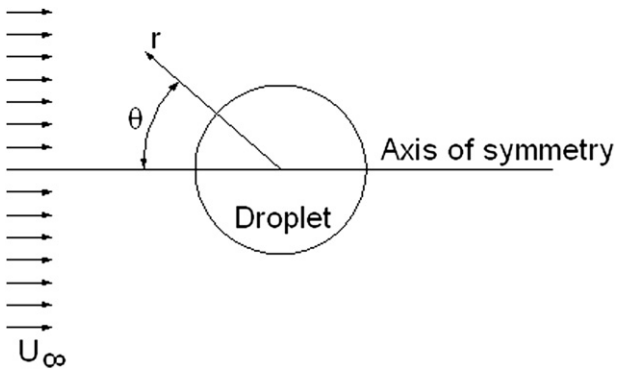

Fig. 1. Problem schematic.

The droplet lifetime (t_d) is defined in the present study as the time it takes the droplet to reach one-tenth of its initial diameter. The average entropy generation rate over the lifetime of the droplet (S') is obtained using the following expression.

$$S' = \frac{1}{t_d}\int_0^{t_d} S dt \tag{46}$$

The individual contributions due to heat transfer, mass transfer, chemical reaction, and coupling between heat and mass transfer can be evaluated using Eq. (46).

4. Results and discussion

The numerical model was used to investigate the rate of entropy generation during the combustion of methanol droplets in dry air at atmospheric pressure. Two separate situations are discussed: A) a suspended droplet with $d_0 = 0.43$ mm, $T_\infty = 300$ K, and $Re_0 = d_0 U_{\infty,0}/\nu_\infty = 0.01$, and B) a moving droplet with $d_0 = 0.5$ mm, $T_\infty = 1200$ K, and initial Reynolds numbers in the range 1–100. This range of initial Reynolds numbers is typical for droplets in practical spray combustion devices such as diesel engines and gas turbines. The initial droplet diameters used for the suspended and moving droplet cases correspond to the diameters used in references [28] and [29], respectively. The freestream velocity is held constant for a suspended droplet, and the low initial Reynolds number (0.01) simulates the nearly quiescent conditions present during "spherically symmetric" microgravity droplet combustion experiments. For a moving droplet, the droplet velocity decreases with time due to the drag force [27].

4.1. Suspended droplet

The rate of entropy generation for suspended droplet combustion with a fixed droplet diameter (0.43 mm), an ambient temperature of 300 K, and an initial Reynolds number of 0.01 is presented. Simulations that include and neglect surface tension effects have been performed and detailed discussions of the numerical results (without studying entropy generation) are available in the literature [28]. Fig. 2 shows the temporal variation of the entropy generation rate due to heat transfer (S_h) (Fig. 2a) and due to chemical reaction (S_r) (Fig. 2b). The entropy generation rate increases sharply till a flame completely envelops the droplet (envelope flame); this takes place around $t = 19.2$ ms and $t = 17.4$ ms when surface tension effects are included and neglected, respectively [28]. The envelope flame becomes nearly spherically symmetric at approximately $t = 40$ ms for both the cases [28]. For the case that includes surface tension effects, the entropy generation rate due to heat transfer (Fig. 2a) reaches a maximum around $t = 70$ ms, and after that it decreases with time. A similar trend is seen for the case without surface tension however, the maximum value of S_h is lower. Surface tension affects the variation of surface water mass fraction as well as surface temperature during the initial stages of combustion [28], which eventually affects the overall gas-phase heat and mass transfer rates, resulting in an increase in the entropy generation rate when surface tension is included. The entropy generation rate due to chemical reaction (Fig. 2b) exhibits a spike and reaches a maximum value around the time when an envelope flame is formed. This spike is caused by the initiation of chemical reactions surrounding the droplet and the subsequent rapid rise in gas-phase temperature. After the spike, S_r decreases with time in a manner similar to S_h. The maximum value of S_h is higher than that of S_r, which is consistent with the literature [37,40].

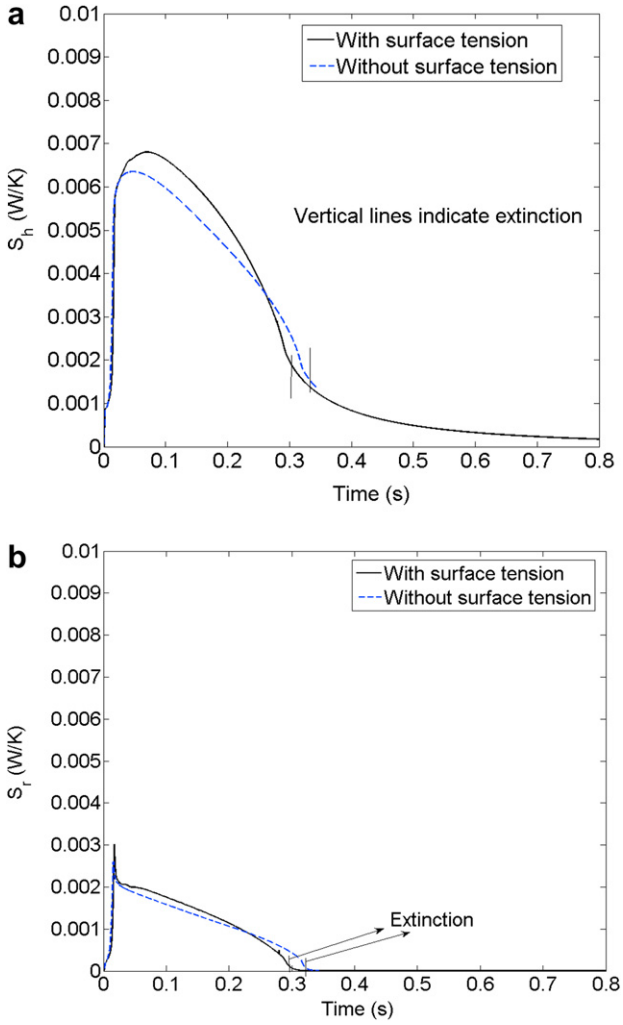

Fig. 2. Entropy generation rate versus time: due to (a) heat transfer, and (b) chemical reaction for suspended droplet.

Fig. 3 shows the temporal variations of the entropy generation rate due to mass transfer (S_m) and the total value (S_t). The entropy generation rate due to mass transfer initially exhibits a sharp increase followed by a gradual decrease. The same trend is observed in the total entropy generation rate as well. The maximum value of S_m (Fig. 3) is much less than that of S_h and S_r (Fig. 2). The results indicate that the entropy generation rate due to coupling between heat and mass transfer (S_c) is approximately three orders of magnitude less than S_h. Thus, S_c can be neglected in the present work which is in agreement with available quasi-steady numerical results [40].

The enhanced internal mixing for the case with surface tension results in greater absorption of water into the droplet [28], which causes the flame to extinguish at an earlier time (see vertical lines in Fig. 2). Extinction occurs at approximately $t = 290$ ms for the case with surface tension, and at approximately $t = 320$ ms when surface tension effects are neglected. After extinction, pure evaporation takes place. The value of S_r is essentially zero after extinction (Fig. 2b), and S_h (Fig. 2a), S_m, and S_t (Fig. 3) decrease with time at a slower rate. Table 1 shows the time-averaged entropy generation rates S'_h, S'_r, S'_m, and S'_t. When the time average is taken over the extinction time, the values are higher for the case that includes surface tension effects. The increase in irreversibilities associated with surface tension effects, along with the decrease in the time to extinction, leads to the higher time-averaged values. The droplet

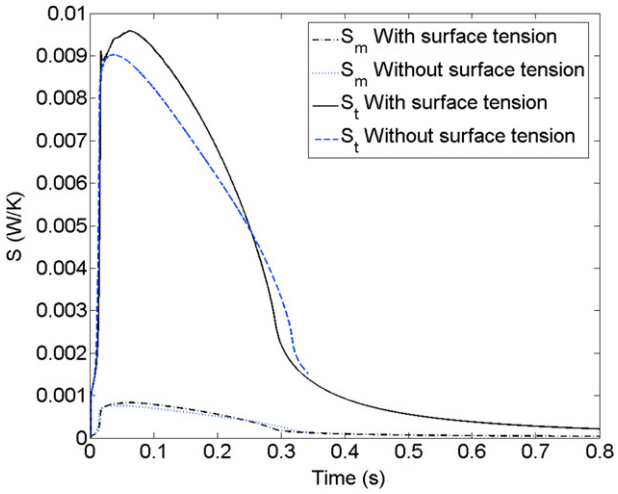

Fig. 3. Entropy generation rate versus time: due to mass transfer (S_m), and the total rate (S_t) for suspended droplet.

diameter at extinction is much higher for the case with surface tension (0.11 mm) when compared to that without (0.054 mm) [28]. After extinction, the droplet diameter slowly decreases due to evaporation in the low-temperature environment (300 K). The droplet lifetime is defined in the present work as the time it takes for the droplet to reach one-tenth of its initial diameter [28], at which time the droplet mass is reduced to 1/1000th of its initial value. The larger extinction diameter leads to a longer droplet lifetime for the case with surface tension (920 ms) when compared to the case without surface tension (340 ms). Thus, as shown in Table 1, the average entropy generation rates over the droplet lifetime are much lower for the case with surface tension than without.

Fig. 4 shows the temporal variations of the ratios $S_r/(S_t-S_r)$ (Fig. 4a) and $S_h/(S_t-S_h)$ (Fig. 4b). The ratio $S_r/(S_t-S_r)$ (Fig. 4a) gradually decreases with time after the initial spike, where it reaches around 0.5, when surface tension effects are both included and neglected. A similar trend in the ratio $S_r/(S_t-S_r)$ is predicted by Hiwase et al. [37] in their one-dimensional simulations for spherically symmetric droplet combustion. The results for the ratio $S_h/(S_t-S_h)$ (Fig. 4b) exhibit a spike to a maximum value of 35 early in the simulations. The large spike in this ratio at the beginning of the simulations is due to the modeling of the external ignition source [27,28]. Unlike the ratio of S_r to (S_t-S_r), the ratio of S_h to (S_t-S_h) gradually increases after the spike until the onset of flame extinction. The ratio $S_h/(S_t-S_h)$ (Fig. 4b) sharply increases during the extinction process, suggesting the increasing importance of irreversibility due to heat transfer during that period. After extinction, the ratio gradually decreases with time.

4.2. Moving droplet

The rate of entropy generation for a moving droplet with a fixed droplet diameter (0.5 mm), and ambient temperature (1200 K) was

Table 1
Average entropy generation rate (W/K) for suspended droplets with and without surface tension effects.

Surface Tension	S'_h	S'_r	S'_m	S'_t
Average over droplet lifetime				
Yes	0.0020	4.23E-04	2.13E-04	0.0026
No	0.0045	0.0011	4.62E-04	0.0061
Average over extinction time				
Yes	0.0051	0.0013	5.44E-04	0.0070
No	0.0045	0.0011	4.73E-04	0.0061

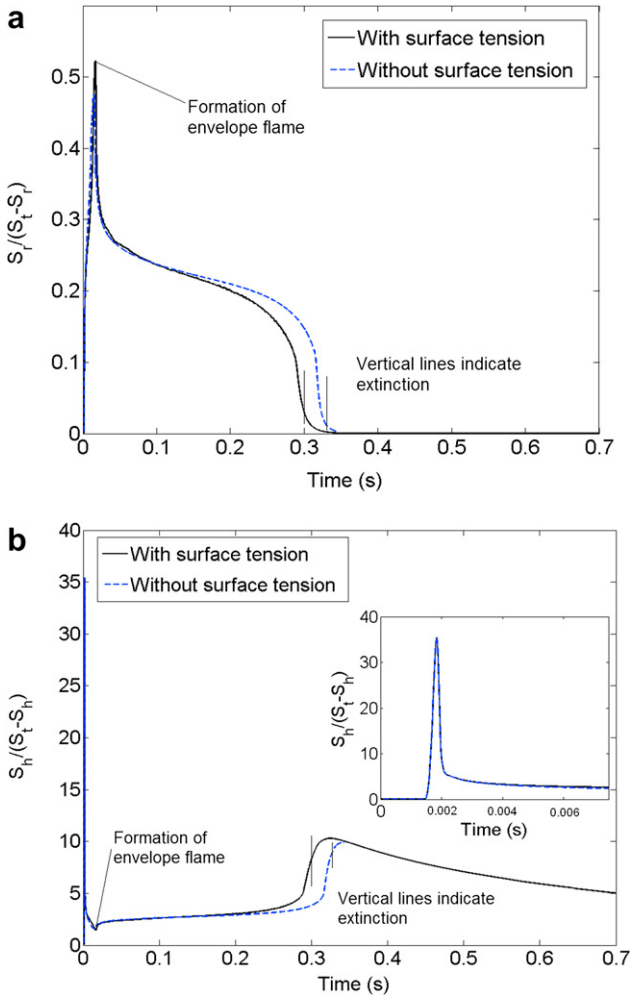

Fig. 4. Temporal variation of (a) $S_r/(S_t-S_r)$ and (b) $S_h/(S_t-S_h)$ for suspended droplet.

also investigated. The initial Reynolds number was varied from 1 to 100, and surface tension effects have been included in the results. Detailed discussions of the combustion characteristics for these simulations (without studying entropy generation) are available in the literature [29]. As in the suspended droplet case, the results for moving droplets indicate that S_c is smaller than S_h by several orders of magnitude.

For the moving droplet simulations, the initial Reynolds number affects the position and shape of the flame formed after the ignition transient and the subsequent behavior of the flame after ignition [29]. The ignition transient occurs over a very short time (compared with the droplet lifetime) at the beginning of the simulations. It consists of the following sequence of events: 1) evaporation and mixing of the fuel vapor and oxidizer, 2) ignition of the fuel vapor/oxidizer mixture downstream of the droplet, and 3) rapid establishment of the flame from the wake region to a size and type (envelope, transition, or wake). At low initial Reynolds numbers, the convective time scale (d/U_∞) is much larger than the chemical reaction time scale, and the flame completely engulfs the droplet (envelope flame). For higher Reynolds numbers, the convective time scale is smaller and the flame may partially surround the droplet (transition flame) or stabilize in the wake of the droplet (wake flame) at the end of the ignition transient. The moving droplet decelerates due to the drag force and its diameter decreases with time. The overall effect is a reduction in the convective time scale which promotes the formation of an envelope flame at some point during the droplet lifetime [27,29]. Once an envelope flame is formed, it remains until extinction.

Fig. 5 shows the variation of S_h with time for the range of initial Reynolds numbers considered. When Re_0 is in the range 1–10 (Fig. 5a), an envelope flame is established very early (at the end of the ignition transient), and the maximum value of S_h increases with Re_0. For Re_0 greater than 10, the maximum value of S_h decreases with an increase in Re_0 (Fig. 5a and b). As Re_0 increases, the droplet must decelerate before an envelope flame is formed, and the time at which an envelope flame is formed also increases [29]. The time it takes to reach the maximum value of S_h also increases with Re_0 (Fig. 5a, corresponding to $Re_0 = 20$ and Fig. 5b), because it is directly related to the time at which an envelope flame is formed [29]. The average value of S_h over the droplet lifetime (S'_h, presented later) is affected by both the maximum value of S_h, and the time it takes to reach that maximum value; a decrease in the maximum value and an increase in the time causes a decrease in S'_h.

Fig. 6 shows the variation of S_r with time for the initial Reynolds numbers considered. The maximum value of S_r increases with Re_0 when Re_0 is less than approximately 10, in a manner similar to S_h (Fig. 5). When Re_0 is increased above 10, the maximum value of S_r decreases slightly and the time it takes to reach the maximum increases (Fig. 6a). For Re_0 greater than approximately 20, there are 2 local maximums in the S_r versus time curves (Fig. 6a and b). At $Re_0 = 20$, the first maximum is lower than the second (Fig. 6a).

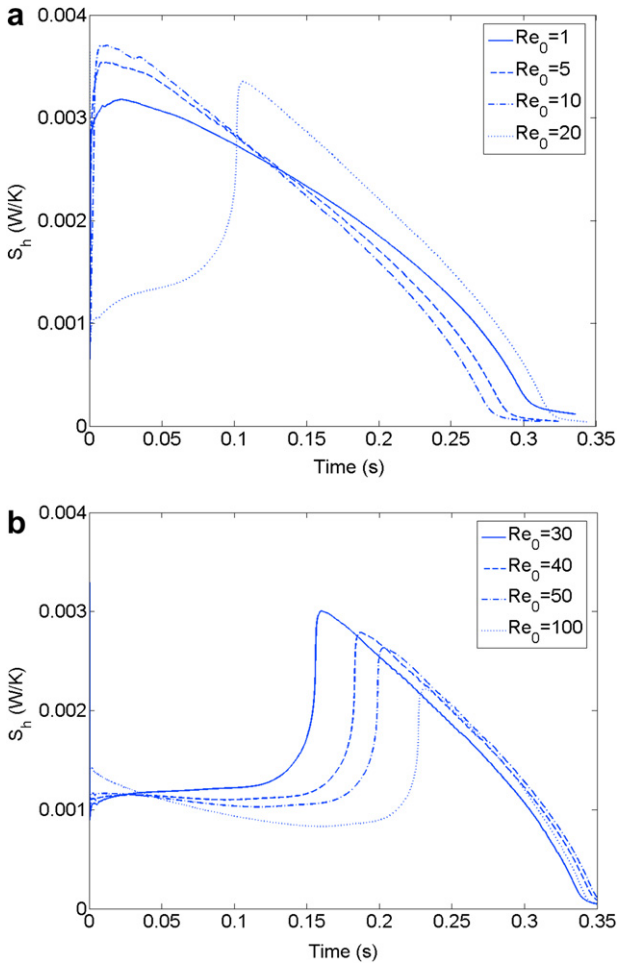

Fig. 5. Entropy generation rate due to heat transfer versus time for Re_0 in the range (a) 1–20, and (b) 30–100 – moving droplet.

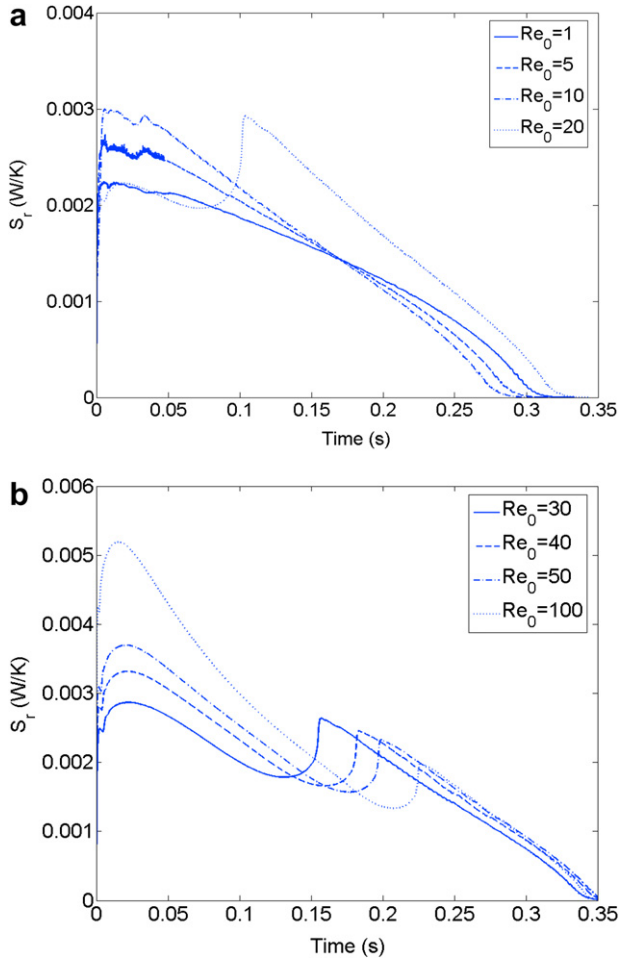

Fig. 6. Entropy generation rate due to chemical reaction versus time for Re_0 in the range (a) 1–20, and (b) 30–100 – moving droplet.

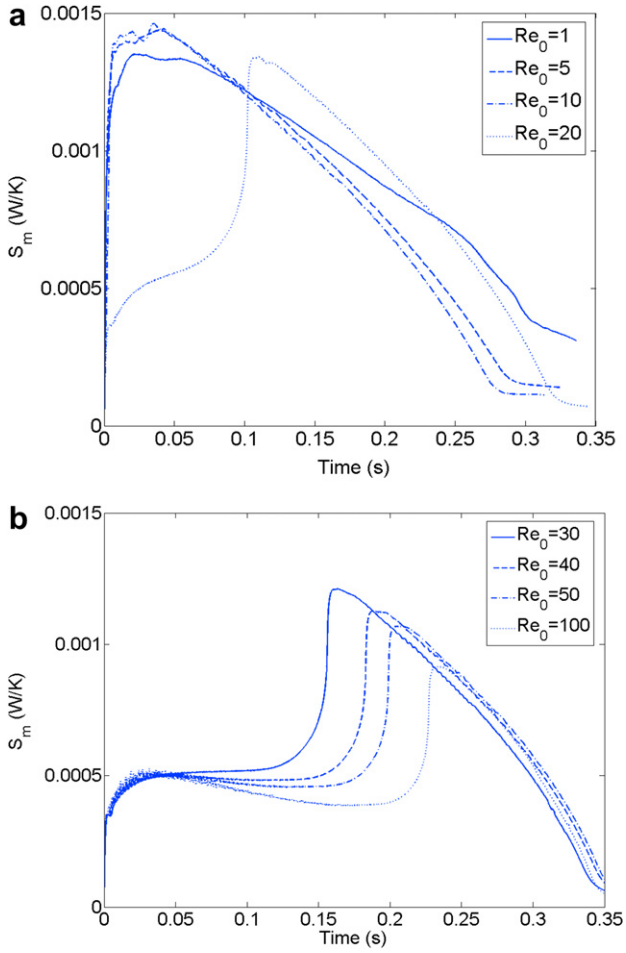

Fig. 7. Entropy generation rate due to mass transfer versus time for Re_0 in the range (a) 1–20, and (b) 30–100 – moving droplet.

The first maximum occurs at the end of the ignition transient, which results in the formation of a wake flame behind the droplet, and its value increases with an increase in Re_0. The first maximum occurs at almost same time (~20 ms) regardless of the initial Reynolds number. However, the second maximum, which occurs during the formation of an envelope flame (different times for different Re_0), has a value that decreases with increasing Re_0. At Re_0 of about 30 (Fig. 6b), the magnitudes of the two local maximums are almost equal. For Re_0 greater than approximately 30, the first of the 2 local maximums has the greater magnitude (Fig. 6b). A comparison of Figs. 5 and 6 shows that the maximum values for S_h are greater than those for S_r at low Re_0, and the maximum values for S_r are greater than those for S_h at high Re_0. Also, in contrast to the results for S_h, the maximum value of S_r increases with Re_0 when Re_0 is between 30 and 100 (Fig. 6b). An increase in the maximum value of S_r, and a decrease in the time it takes to reach that maximum value, would tend to increase the average value of S_r over the droplet lifetime (S'_r, presented later).

Fig. 7 shows the variation of S_m with time for the initial Reynolds numbers considered. The results are qualitatively similar to those obtained for S_h (Fig. 5). Thus, the discussion regarding the average value over the droplet lifetime associated with Fig. 5 is applicable to Fig. 7. The maximum values for S_m are much lower than the maximum values for S_h. A similar result was obtained for the low ambient temperature (300 K) suspended droplet case presented earlier; predicted maximum values for S_m were much lower than the values for S_h (compare Figs. 2a and 3, averaged values in Table 1). As the ambient temperature increases, the entropy generation due to mass transfer also increases (presented later) because of the larger values for diffusion coefficients. This is consistent with results available in the literature [40]. The maximum values for S_m in Fig. 7 correspond to the formation of an envelope flame.

Fig. 8 shows the variation of the S_t with time for the initial Reynolds numbers considered. The temporal variation of S_t (Fig. 8a) is similar to S_h (Fig. 5a), S_r (Fig. 6a), and S_m (Fig. 7a) when Re_0 is less than or equal to 10. When Re_0 is increased beyond 10, the maximum value of S_t decreases slightly (Fig. 8a, corresponding to $Re_0 = 20$) and the time taken to reach the maximum also increases as observed in S_h, S_m and S_r. For Re_0 greater than 20, S_t (Fig. 8b) exhibits the 2 local maximums associated with S_r (Fig. 6b). The change in S_t between $Re_0 = 20$ and 30 indicates that the entropy generation rate due to chemical reaction begins to dominate the total entropy generation rate in this range of initial Reynolds number. Thus, unlike the low ambient temperature (300 K) and low Re_0 (0.01) case considered earlier, S_r is more important than S_h in contributing to S_t in these high ambient temperature and high Re_0 cases.

As mentioned in the discussions of Figs. 5, 6 and 7 the maximum entropy generation rate, and the time it takes to reach the maximum, both have an effect on the average entropy generation rate over the droplet lifetime. The droplet lifetime also affects the average entropy generation rate; an increase in t_d tends to cause a decrease in S'. The droplet lifetimes for the moving droplet cases used in the present

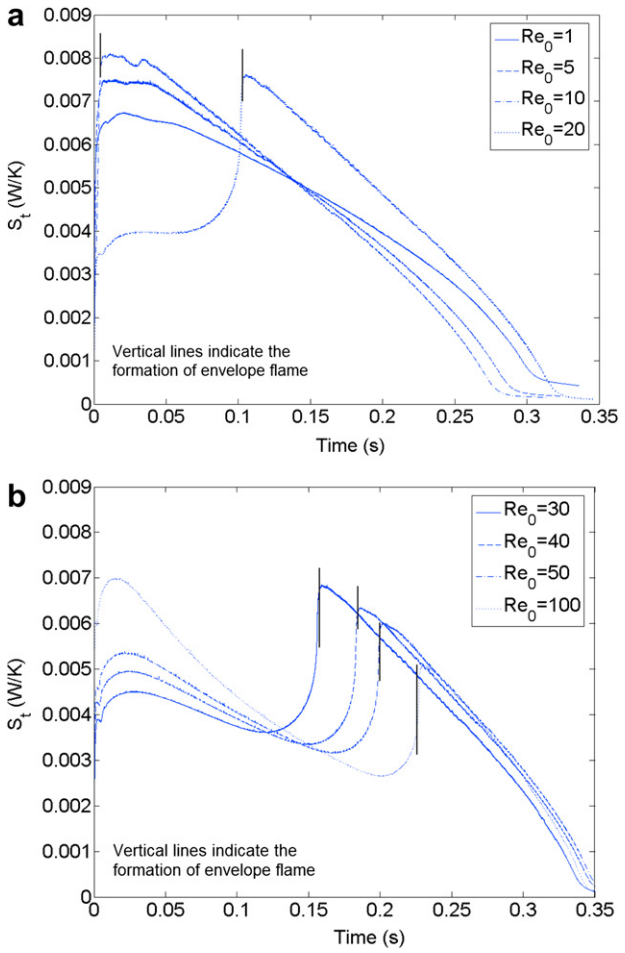

Fig. 8. Total entropy generation versus time for Re_0 in the range (a) 1–20, and (b) 20–100 – moving droplet.

work have been presented by Raghavan et al. [29]. They identified three distinct ranges of Re_0 to describe the trends in droplet lifetime. As Re_0 increases, the droplet lifetime first decreases when $Re_0 < 10$, then t_d increases in the range $10 < Re_0 < 15$, and finally, t_d decreases for $Re_0 > 15$ [29]. A comparison of the trends in droplet lifetime with

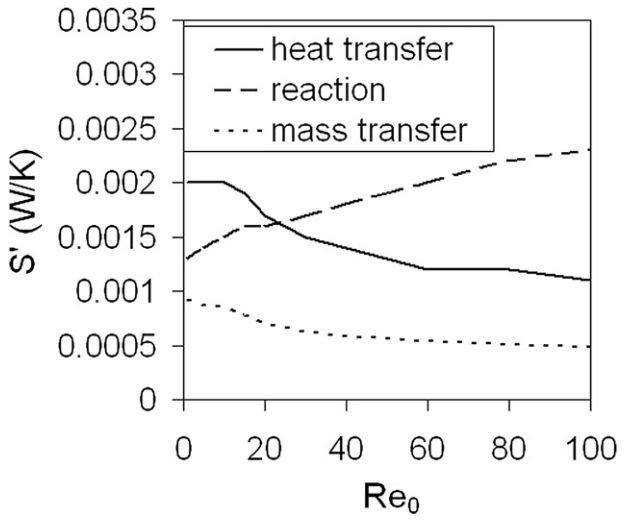

Fig. 9. Average entropy generation rate due to heat transfer, mass transfer, and chemical reaction versus Re_0 – moving droplet.

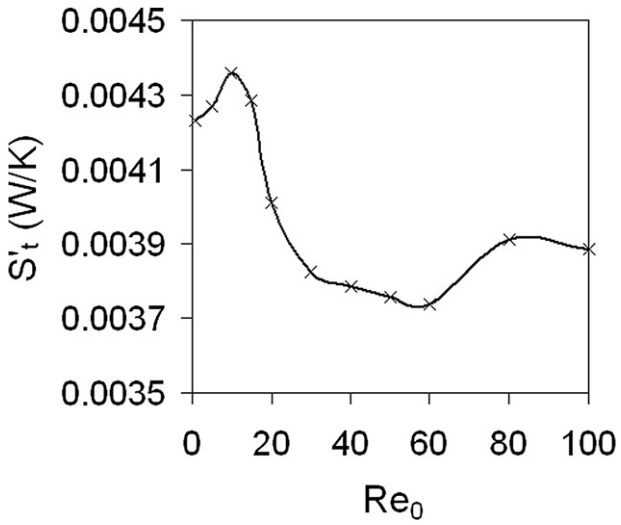

Fig. 10. Average entropy generation rate versus Re_0 – moving droplet.

the trends in Figs. 5, 6 and 7 shows that the three factors (maximum value, time to maximum value, and droplet lifetime) compete with each other to produce a net effect on the average entropy generation rate.

Fig. 9 shows the average entropy generation rates S'_h, S'_m and S'_r as a function of Re_0. The values for S'_h and S'_m are practically constant when Re_0 is less than or equal to 10 due to the formation of an envelope flame early in the droplet lifetime. When Re_0 is greater than 10, S'_h and S'_m both decrease as Re_0 increases. The value for S'_r increases with Re_0, and for Re_0 greater than approximately 20, S'_r becomes greater than S'_h. Fig. 9 also indicates that S'_m is the smallest of the three contributors to S'_t over the entire range of initial Reynolds numbers considered.

Fig. 10 shows the variation of the average entropy generation rate (S'_t) with Re_0. The variation between the minimum and maximum values of S'_t shown in the figure is less than 20%. There is an increasing trend in S'_t with Re_0 until Re_0 is approximately equal to 10. At low Re_0, the values for S'_h and S'_m are almost constant and S'_r increases resulting in an increase in S'_t. The value of S'_t decreases with an increase in Re_0 in the range $Re_0 = 10$ to 50 due to the decrease in S'_h and S'_m. For Re_0 greater than 60, S'_t increases with Re_0 due to the increase in S'_r. The numerical predictions presented in Fig. 10 clearly indicate that, for the combustion of moving methanol droplets, an initial Reynolds number of approximately 55 results in a minimum average entropy generation rate.

5. Conclusions

A detailed derivation for the volumetric rate of entropy generation in a multi-component reacting mixture of ideal gases has been presented. The gas-phase entropy generation rate during methanol droplet combustion in a low-pressure, zero-gravity environment was studied using a transient, axisymmetric numerical model. Results for a suspended droplet with a low ambient temperature (300 K) and a low initial Reynolds number (0.01), and a moving droplet with a high ambient temperature (1200 K) and a range of initial Reynolds numbers (1–100) were presented. The effect of surface tension on the entropy generation rate was investigated for the suspended droplet case.

The suspended droplet results show that the average entropy generation rate over the droplet lifetime is higher for the case that neglects surface tension effects. Neglecting surface tension effects

produces a smaller extinction diameter, and therefore a shorter droplet lifetime and higher average entropy generation rate. The low ambient temperature employed results in a lower mass transfer contribution to the average entropy generation rate. Heat transfer is the highest contributor to the entropy generation rate, followed by chemical reaction, and finally mass transfer. Both the suspended and the moving droplet results indicated that coupling between heat and mass transfer has a negligible contribution to the entropy generation rate.

In the moving droplet case, entropy generation due to both heat transfer and mass transfer decreases, and entropy generation due to chemical reaction increases, with an increase in initial Reynolds number. The heat transfer and chemical reaction contributions to the entropy generation rate were greater than the contribution of mass transfer over the entire range of initial Reynolds numbers considered. Chemical reactions have a smaller effect on the entropy generation rate than heat transfer at low initial Reynolds numbers and a larger effect at high initial Reynolds numbers. For moving droplets, the average entropy generation rate over the droplet lifetime presents a minimum value at an initial Reynolds number of approximately 55.

Acknowledgements

This research was partially funded by NASA EPSCoR under grant NCC5-572. Computational resources were provided by the Thermal-Fluids computational facility and the Research Computing Facility at the University of Nebraska – Lincoln.

Appendix A

The governing equations for the gas and liquid phases are the transient axisymmetric equations for continuity, conservation of species, conservation of energy and conservation of momentum, in $r-\theta$ spherical coordinates. In the liquid phase, which consists of a binary methanol-water system, there is no production or destruction of species. A set of interfacial conservation equations couple the gas and the liquid phases.

The gas-phase energy conservation equation employed in the present study is given below:

$$\frac{\partial}{\partial t}(\rho T)+\nabla\cdot(\rho \boldsymbol{v} T) = \nabla\cdot\left(\frac{k}{c_p}\nabla T\right)+\frac{k}{c_p^2}\nabla T\cdot\nabla c_p - \frac{1}{c_p}\sum_{i=1}^{N}\omega_i h_i-\frac{\rho}{c_p}\sum_{i=1}^{N}Y_i\boldsymbol{V}_i\cdot\nabla h_i \tag{A1}$$

The gas phase and the liquid phase are coupled at the interface. The gas and liquid phases are constrained to have the same temperature at the interface ($T_{g,s}=T_{l,s}$), and the no-slip condition is employed to relate the tangential velocities at the interface ($v_{\theta,g,s}=v_{\theta,l,s}$). Conservation of mass at the interface yields the radial velocity component (v_r), given as follows:

$$\rho_{g,s}\left(v_{r,g,s}-\frac{dR}{dt}\right) = \rho_{l,s}\left(v_{r,l,s}-\frac{dR}{dt}\right) \tag{A2}$$

In the above equation (dR/dt) represents the droplet regression rate. Conservation of species at the interface is given by the following expressions.

$$\text{Fuel}: \ m''_\theta Y_{f,g,s}+\rho_{g,s}Y_{f,g,s}V_{r,f,g,s}=m''_\theta Y_{f,l,s}+\rho_{l,s}Y_{f,l,s}V_{r,f,l,s} \tag{A3}$$

$$\text{Water}: \ m''_\theta Y_{w,g,s}+\rho_{g,s}Y_{w,g,s}V_{r,w,g,s} = m''_\theta Y_{w,l,s}+\rho_{l,s}Y_{w,l,s}V_{r,w,l,s} \tag{A4}$$

$$\text{For other species}: \ m''_\theta Y_{i,g,s}+\rho_{g,s}Y_{i,g,s}V_{r,i,g,s} = 0 \tag{A5}$$

Conservation of energy at the interface is given by

$$m''_\theta\left(Y_{f,l,s}L_f+Y_{w,l,s}L_w\right)+\rho_{l,s}\left(Y_f V_{r,f}L_f+Y_w V_{r,w}L_w\right)_{l,s} - \left(k_{g,s}\frac{dT}{dr}\bigg|_{g,s}\right) = -k_{l,s}\frac{dT}{dr}\bigg|_{l,s} \tag{A6}$$

The equation for continuity of shear stress at the interface is of particular interest for the present study and includes surface tension effects. It is given by,

$$\mu_{g,s}\left[\frac{\partial v_\theta}{\partial r}+\frac{1}{r}\frac{\partial v_r}{\partial\theta}-\frac{v_\theta}{r}\right]_{g,s}+\frac{1\partial\sigma_T}{r\ \partial\theta}\bigg|_s=\mu_{l,s}\left[\frac{\partial v_\theta}{\partial r}+\frac{1}{r}\frac{\partial v_r}{\partial\theta}-\frac{v_\theta}{r}\right]_{l,s} \tag{A7}$$

where the second term on the left-hand side is the surface tension gradient along the droplet surface. The gas-phase diffusion velocities, which depend upon concentration and temperature gradients for all N species, are solved according to the method presented by Pope and Gogos [19]. The liquid phase consists of a binary mixture of methanol and water, and the diffusion velocities are calculated using Fick's Law for ordinary diffusion alone. The binary diffusion coefficient is calculated as a function of mutual binary diffusion coefficients at very low concentrations, mole fractions of the species and a thermodynamic correction factor that depends upon composition and temperature for a binary mixture. The interface composition is determined using a low-pressure binary vapor–liquid equilibrium equation based upon the activity coefficients. The activity coefficients are calculated using the Wilson correlation [42]. Variable thermo-physical properties in the gas phase are calculated using correlations from Reid et al. [43] and McBride et al. [44]. The liquid-phase properties are calculated using correlations from Reid et al. [43] as well as Teja [45] and Teja and Rice [46]. Surface tension for a pure component (methanol or water) is calculated from a temperature dependent curve-fit of experimental data [47]. A mixing rule based on composition [43] is used to yield a temperature and composition dependent surface tension. Thus, both the droplet surface composition and the droplet surface temperature play a role in determining surface tension. The experimental results of Santos et al. [48] for water/methanol mixtures in thermodynamic equilibrium with air at 303.15 K along with results from the code used in this study compare well.

A one-step overall reaction is used to model the combustion of methanol in air and is given below:

$$CH_3OH+1.5(O_2+3.77N_2)\rightarrow CO_2+2H_2O+1.5(3.77N_2) \tag{A8}$$

The resulting expression for the mass-based rate of production/destruction of species i per unit volume, given by ω_i, is written as:

$$\omega_i = W_i(v''_i-v'_i)A\left(\frac{\rho Y_f}{W_f}\right)^a\left(\frac{\rho Y_o}{W_o}\right)^b\exp\left[\frac{-E_a}{R_u T}\right] \tag{A9}$$

The pre-exponential factor (A), activation energy (E_a) and the fuel and oxygen concentration exponents (a and b) used in the simulation have been taken from Westbrook and Dryer [49].

The governing equations are discretized using the finite volume [50] and SIMPLEC [51] methods. Convection-diffusion is modeled using the power-law scheme [50]. A collocated grid is used with hyperbolic tangent stretching functions [52] used to cluster the grid

points near the droplet surface in both the gas and the liquid phases. The discretized equations are solved using the Alternating Direction Implicit (ADI) method with the Tri-Diagonal Matrix Algorithm (TDMA). Iterations are performed within each time step until desired convergence is achieved. An adaptive time step has also been employed. Grid and domain independence studies have been carried out to ensure that the solution is independent of grid and domain size. The minimum and maximum time steps have been fixed so as to capture the physics during the entire evaporation and combustion processes.

Additional Nomenclature for Appendix A

A	pre-exponential factor
a	fuel concentration exponent in reaction equation
b	oxygen concentration exponent in reaction equation
E_a	activation energy
L	latent heat of vaporization
m''_θ	local mass flux at the droplet surface
R	droplet radius
V	diffusion velocity (scalar component)
v	velocity (scalar component)

Greek Symbols

ν'_i	stoichiometric coefficient of the ith species as a reactant
ν''_i	stoichiometric coefficient of the ith species as a product
σ_T	surface tension

Subscripts

f	fuel
g	gas-phase
l	liquid-phase
r	radial direction
s	droplet surface
w	water

References

[1] S. Kumagai, H. Isoda, Combustion of fuel droplets in a falling chamber, in: Proceedings of the Combustion Institute, vol. 6. The Combustion Institute, Pittsburgh, PA, 1957 pp. 726–731.

[2] S. Kumagai, T. Sakai, S. Okajima, Combustion of free fuel droplets in a freely falling chamber. Proceedings of the Combustion Institute 13 (1971) 779–785.

[3] S.Y. Cho, M.Y. Choi, F.L. Dryer, Extinction of a free methanol droplet in microgravity. Proceedings of the Combustion Institute 23 (1990) 1611–1617.

[4] J.C. Yang, G.S. Jackson, C.T. Avedisian, Combustion of unsupported methanol/dodecanol mixture droplets at low gravity. Proceedings of the Combustion Institute 23 (1990) 1619–1625.

[5] A. Lee, C.K. Law, An experimental investigation on the vaporization and combustion of methanol and ethanol droplets. Combustion Science and Technology 86 (1992) 253–265.

[6] H. Hara, S. Kumagai, The effect of initial diameter on free droplet combustion with spherical flame. Proceedings of the Combustion Institute 25 (1994) 423–430.

[7] D.L. Dietrich, J.B. Haggard Jr., F.L. Dryer, V. Nayagam, B.D. Shaw, F.A. Williams, Droplet combustion experiments in space lab. Proceedings of the Combustion Institute 26 (1996) 1201–1207.

[8] A.J. Marchese, F.L. Dryer, R.O. Colantonio, V. Nayagam, Microgravity combustion of methanol and methanol/water droplets: droplet tower experiments and model predictions. Proceedings of the Combustion Institute 26 (1996) 1209–1217.

[9] A.J. Marchese, F.L. Dryer, R.O. Colantonio, Radiative effects in space-based methanol/water droplet combustion experiments. Proceedings of the Combustion Institute 27 (1998) 2627–2634.

[10] K. Okai, O. Moriue, M. Araki, M. Tsue, M. Kono, J. Sato, D.L. Dietrich, F.A. Williams, Pressure effects on combustion of methanol and methanol/Dodecanol single droplets and droplet pairs in microgravity. Combustion and Flame 121 (No. 3) (2000) 501–512.

[11] B.D. Shaw, Studies of influences of liquid-phase species diffusion on spherically symmetric combustion of miscible binary droplets. Combustion and Flame 81 (Nos. 3–4) (1990) 277–288.

[12] B.L. Zhang, J.M. Card, F.A. Williams, Application of rate-ratio asymptotics to the prediction of extinction for methanol droplet combustion. Combustion and Flame 105 (No. 3) (1996) 267–290.

[13] A.J. Marchese, F.L. Dryer, The effect of liquid mass transport on the combustion and extinction of bi-component droplets of methanol and water. Combustion and Flame 105 (Nos. 1–2) (1996) 104–122.

[14] H. Sami, M. Ogasawara, Study on the burning of a fuel drop in heated and pressurized air stream. Bulletin of the Japan Society of Mechanical Engineers 13 (No. 57) (1970) 395–404.

[15] S.R. Gollahalli, T.A. Brzustowski, Experimental studies on the flame structure in the wake of a burning droplet. Proceedings of the Combustion Institute 14 (1973) 1333–1344.

[16] H.A. Dwyer, B.R. Sanders, A detailed study of burning fuel droplets. Proceedings of the Combustion Institute 21 (1986) 633–639.

[17] P. Balakrishnan, T. Sundararajan, R. Natarajan, Interference effects during burning of tandem porous spheres in mixed convective environment. AIAA Journal 38 (2000) 1889–1898.

[18] P. Balakrishnan, T. Sundararajan, R. Natarajan, Combustion of a fuel droplet in a mixed convective environment. Combustion Science and Technology 163 (2001) 77–106.

[19] D.N. Pope, G. Gogos, A new multi-component diffusion formulation for the finite volume method: application to convective droplet dombustion. Numerical Heat Transfer Part B 48 (No. 3) (2005) 213–234.

[20] D.N. Pope, G. Gogos, Numerical simulation of fuel droplet extinction due to forced convection. Combustion and Flame 142 (Nos. 1–2) (2005) 89–106.

[21] V. Raghavan, V. Babu, T. Sundararajan, R. Natarajan, Flame shapes and burning rates of spherical fuel particles in a mixed convective environment. International Journal of Heat and Mass Transfer 48 (Nos. 25–26) (2005) 5354–5370.

[22] I. Aharon, B.D. Shaw, Marangoni instability of bi-component droplet gasification. Physics of Fluids 8 (No. 7) (1996) 1820–1827.

[23] H.A. Dwyer, I. Aharon, B.D. Shaw, H. Niazmand, Surface tension influences on methanol droplet vaporization in the presence of water. Proceedings of the Combustion Institute 26 (1996) 1613–1619.

[24] H.A. Dwyer, B.D. Shaw, H. Niazmand, Droplet/flame interactions including surface tension influences. Proceedings of the Combustion Institute 27 (1998) 1951–1957.

[25] H.A. Dwyer, B.D. Shaw, Marangoni and stability studies on fiber-supported methanol droplets evaporating in reduced gravity. Combustion Science and Technology 162 (2001) 331–346.

[26] A.T. Shih, C.M. Megaridis, Thermocapillary flow effects on convective droplet evaporation. International Journal of Heat and Mass Transfer 39 (No. 2) (1996) 247–257.

[27] D.N. Pope, D. Howard, K. Lu, G. Gogos, Combustion of moving droplets and suspended droplets: transient numerical results. AIAA Journal of Thermophysics and Heat Transfer 19 (No. 3) (2005) 273–281.

[28] V. Raghavan, D. Howard, D.N. Pope, G. Gogos, Surface tension effects during low Reynolds number methanol droplet combustion. Combustion and Flame 145 (2006) 791–807.

[29] V. Raghavan, D.N. Pope, G. Gogos, Effects of forced convection and surface tension during methanol droplet combustion. AIAA Journal of Thermophysics and Heat Transfer 20 (No. 4) (2006) 787–798.

[30] J.O. Hirschfelder, C.F. Curtiss, R.B. Bird, Molecular Theory of Gases and Liquids. Wiley, New York, 1954.

[31] A. Bejan, The thermodynamic design of heat and mass transfer processes and devices. International Journal of Heat and Fluid Flow 8 (1987) 258–276.

[32] J.Y. San, W.M. Worek, Z. Lavan, Entropy generation in convective heat transfer and isothermal convective mass transfer. Transactions of the ASME, Journal of Heat Transfer 109 (1987) 647–652.

[33] C.G. Carrington, Z.F. Sun, Second law analysis of combined heat and mass transfer phenomena. International Journal of Heat and Mass Transfer 34 (No. 11) (1991) 2767–2773.

[34] V.S. Arpaci, A. Selamet, Entropy production in flames. Combustion and Flame 73 (1988) 251–259.

[35] S.K. Dash, S.K. Som, Transport processes and associated irreversibilities in droplet combustion in a convective medium. International Journal of Energy Research 15 (No. 7) (1991) 603–619.

[36] I.K. Puri, Second law analysis of convective droplet burning. International Journal of Heat and Mass Transfer 35 (No. 10) (1992) 2571–2578.

[37] S. Hiwase, A. Datta, S.K. Som, Entropy balance and exergy analysis in the process of droplet combustion. Journal of Physics D: Applied Physics 31 (1998) 1601–1610.

[38] A. Datta, S.K. Som, Thermodynamic irreversibilities and second law analysis in a spray combustion process. Combustion Science and Technology 142 (1999) 29–54.

[39] K. Nishida, T. Takagi, S. Kinoshita, Analysis of entropy generation and exergy loss during combustion. Proceedings of the Combustion Institute 29 (2002) 869–874.

[40] V. Raghavan, G. Gogos, V. Babu, T. Sundararajan, Entropy generation during the quasi-steady combustion of spherical fuel particles. International Journal of Thermal Sciences 46 (No. 6) (2007) 589–604.

[41] F.A. Williams, Combustion Theory, second ed. Benjamin/Cummings, Menlo Park, CA, 1985.
[42] K. Kurihara, M. Nakamichi, K. Kojima, Isobaric vapor–liquid equilibria for the methanol + ethanol + water and the three constituent binary systems. Journal of Chemical and Engineering Data 38 (1993) 446–449.
[43] R.C. Reid, J.M. Prausnitz, B.E. Poling, The Properties of Gases and Liquids. McGraw-Hill Inc., New York, 1987.
[44] B.J. McBride, G. Sanford, M.A. Reno, Coefficients for calculating thermodynamic and transport properties of individual species. NASA, TM 4513 (1993).
[45] A.S. Teja, Simple method for the calculation of heat capacities of liquid mixtures. American Chemical Engineering Society 28 (1983) 83–85.
[46] A.S. Teja, P. Rice, Generalized corresponding states method for the viscosities of liquid mixtures. Industrial and Engineering Chemistry Fundamentals 20 (No. 1) (1981) 77–81.
[47] N.B. Vargaftik, Y.K. Vinogradov, V.S. Yargin, Handbook of Physical Properties of Liquids and Gases: Pure Substances and Mixture. Begell House, Inc., New York, 1996.
[48] B.M.S. Santos, A.G.M. Ferriera, I.M.A. Fonseca, Surface and interfacial tensions of the systems water + n-Butyl Acetate + methanol and water + n-Pentyl Acetate + methanol at 303.15 K. Fluid Phase Equilibria 208 (2003) 1–21.
[49] C.H. Westbrook, F.L. Dryer, Simplified reaction mechanisms for the oxidation of hydrocarbon fuels in flames. Combustion Science Technology 27 (1981) 31–43.
[50] S.V. Patankar, Numerical Heat Transfer and Fluid Flow. Hemisphere, New York, 1980.
[51] J.P. Van Doormal, G.D. Raithby, Enhancements of the SIMPLE method for predicting incompressible fluid flows. Numerical Heat Transfer 7 (1984) 147–163.
[52] M. Vinokur, On one-dimensional stretching functions for finite-difference calculations. Journal of Computational Physics 50 (1983) 215–234.